



Effect of hydrostatic pressure on opto-electronic, elastic and thermoelectric properties of the double perovskites Rb_2SeX_6 ($X=\text{Cl}, \text{Br}$): a DFT study[☆]

A. A. Yahaya^{id}^{a,b,*}, W. A. Yahya^{id}^a, I. A. Rahmon^a

^aDepartment of Physics and Materials Science, Kwara State University, Malete, Nigeria

^bDepartment of Physics, Kebbi State University of Science and Technology, Aliero, Nigeria

Abstract

Double perovskites find applications across a diverse range of situations and varying pressure conditions. In this work, Quantum ESPRESSO code with a plane wave basis set was used to study the opto-electronic, elastic, and thermoelectric properties of Rb_2SeX_6 ($X=\text{Cl}, \text{Br}$) double perovskites under hydrostatic pressure (0 - 8 GPa). Perdew-Burke-Ernzerhof for Solids (PBEsol) with generalized gradient approximation (GGA) was used as exchange-correlation functional. The band gap values of the materials decrease under hydrostatic pressure. Rb_2SeCl_6 has a band gap value of 2.44 eV at 0 GPa, 2.21 eV at 2 GPa. Above 2 GPa, the material has a metallic nature. Rb_2SeBr_6 has a band gap value of 1.56 eV at 0 GPa, but has a metallic nature under hydrostatic pressure (2 GPa to 8 GPa). The optical properties results indicate that the materials exhibit maximum absorption, high reflectivity, low optical loss in the visible and ultraviolet regions, good optical conductivity, and a refractive index suitable for use in opto-electronic applications. The materials are confirmed to be mechanically stable under all the hydrostatic pressure values studied. Electrical conductivity, thermal conductivity, and Seebeck coefficient (S) values of the studied materials increase with an increase in hydrostatic pressure and temperature. The maximum value of S for Rb_2SeBr_6 is 0.248×10^3 (m V/k), while for Rb_2SeCl_6 , maximum $S = 0.175 \times 10^3$ (m V/k). The positive values of S suggest that the predominant charge carriers of $\text{Rb}_2\text{SeCl}_6/\text{Br}_6$ are holes. Also, Rb_2SeBr_6 has a figure of merit (ZT) value of 3.44, while for Rb_2SeCl_6 , $ZT = 1.07$. Since the values of ZT are greater than unity, the two double perovskite materials have good ZT values for thermoelectric device engineering. The results also suggest that Rb_2SeBr_6 is a better thermoelectric material than Rb_2SeCl_6 .

DOI:10.46481/asr.2024.3.1.171

Keywords: Hydrostatic pressure, Density functional theory, Double perovskite, Opto-electronic property, Thermoelectric property

Article History :

Received: 10 November 2023

Received in revised form: 28 January 2024

Accepted for publication: 10 February 2024

Published: 20 February 2024

© 2024 The Author(s). Published by the Nigerian Society of Physical Sciences under the terms of the Creative Commons Attribution 4.0 International license. Further distribution of this work must maintain attribution to the author(s) and the published article's title, journal citation, and DOI.

1. Introduction

The application of hydrostatic pressure has proven to be a useful tool for adjusting the structural phases and photovoltaic characteristics of hybrid perovskites [1, 2]. By altering the energy landscapes and charge-carrier dynamics of halide perovskites, applied pressure reveals unexpected characteristics. Compressed halide perovskites exhibit better solar performance due to the optimized band gap, extended charge-carrier lifetimes, decreased trap-state densities, and adjusted carrier conductivities [1, 2].

*Corresponding author: Tel.: +234-703-989-9267;

Email address: yahyaabubakaraliero@gmail.com (A. A. Yahaya^{id})

The association between a material's band structure and conductivity [3] demonstrates the connection between crystal structure, optical and electrical properties. A material's electrical band structure is inextricably tied to the arrangement of atoms within its crystal lattice. Pressure causes the lattice to compress, reducing atomic spacing inside the material [4]. This compression significantly affects the energy levels of the valence and conduction bands, as well as the overlap of atomic orbitals [4]. Several phenomena, including quantum confinement, changes in electronic states, and momentum disparities, can account for the observed variations in the energy band gap. Under hydrostatic pressure, interatomic distances decrease, leading to closer atomic proximity [4]. According to Ahmad *et al.* [4], quantum confinement effects may intensify, potentially altering the effective size of electronic wavefunctions. The energy band gap widens as the energy difference between the conduction and valence bands increases. Pressure-induced changes in atomic arrangements can produce changes in the positions of electronic states, which can impact the energy of the bands [4]. To foresee a material's potential applications and device performance in opto-electronics and photovoltaics (PVs), its optical properties must be understood. The frequency-dependent complex dielectric function describes the optical transition between occupied and unoccupied orbitals [5]. Dielectric functions can be used to analyze the absorption coefficient $I(\omega)$, reflectivity $R(\omega)$, energy loss $L(\omega)$, conductivity $\text{Re}(\sigma)$, extinction coefficients $K(\omega)$, and complex refractive index $n(\omega)$.

When pressure is applied to a material, the interatomic distances inside it change, resulting in changes in lattice properties [4]. As a result, structural properties change in response to pressure, largely due to alterations in elastic constants. These elastic constants are closely related to mechanical properties, indicating that hydrostatic pressure influences the mechanical behavior of the material. It's also worth noting that mechanical properties are closely related to electronic properties. Materials with stronger covalent bonds typically have higher Young's moduli than those with weaker metallic linkages [4]. The "stress-strain" technique, commonly implemented in the Quantum Espresso code [6, 7], is used to calculate the independent elastic constants, which are crucial for understanding the characteristics of solid compounds. Thermoelectric materials transform waste energy (heat) from any system into electrical energy [8–10]. Thermoelectric materials could be used to make energy gadgets, generate electricity, and cooling devices. The transport qualities of designed compositions are investigated to see whether they are appropriate for that use. To improve thermoelectric efficiency, materials must have high Seebeck coefficient (S), electrical conductivity (σ/τ), power factor (PF), and figure of merit (ZT), while thermal conductivity (κ_e/τ) must be low [9, 11]. Other factors influencing thermoelectric efficiency include increased carrier mobility and smaller band gaps [9].

The electronic, optical, elastic, and thermoelectric properties of Rb_2SeX_6 ($X=\text{Br}, \text{Cl}$) have been carried out by Yahya *et al.* [10]. The calculated band gap values of Rb_2SeBr_6 were 1.7574 and 1.569 eV using GGA-PBE and GGA-PBESol, respectively, and are strikingly close to those of the two most used inorganic/organic perovskites, viz., FAPbI_3 and MAPbI_3 . The optical properties such as refractive index, absorption coefficients, electron energy loss, conductivity, and reflectivity computed in the study lead to the conclusion that Rb_2SeX_6 ($X=\text{Br}, \text{Cl}$) are semiconductor materials with good electron generation values and have high potential applications in the opto-electronic industry. $\text{Rb}_2\text{SeBr}_6/\text{Cl}_6$ shear anisotropy values of 3.09 and 1.71, respectively, which indicate that they are isotropic in nature. The materials' computed Poisson's ratios of 0.32 and 0.26 indicate that they are ductile materials. They exhibit p-type conduction, as evidenced by the positive computed values of the Seebeck coefficient, and they have figure of merit values (ZT) that is greater than one, indicating that they are effective thermoelectric materials.

In Ref. [12], 42 inorganic double perovskite materials were examined using density functional theory (DFT). The analysis of high-throughput computing data was introduced using the data mining technique in informatics, starting with the fabrication of double perovskite crystal structures. The findings reveal that 39 of the crystals have stable perovskite structures. The materials were found to be mechanically stable. Li *et al.* [13] also used theoretical methods to study the mechanical, structural, and opto-electronic properties of A_2SeX_6 ($A=\text{Rb}, \text{K}; X=\text{Cl}, \text{Br}, \text{I}$) lead-free double perovskites. The outcome of the calculations suggests that A_2SeX_6 ($A=\text{Rb}, \text{K}; X=\text{Cl}, \text{Br}, \text{I}$) double perovskite materials are ductile and mechanically stable.

In the previous theoretical studies on Rb_2SeX_6 ($X=\text{Cl}, \text{Br}, \text{I}$), the properties were calculated at 0 GPa [10, 12, 13]. Perovskite materials have applications in a variety of situations within a range of pressure values; therefore, the study of materials' properties under hydrostatic pressure is essential. In the current study, opto-electronic, elastic, and thermoelectric properties of Rb_2SeX_6 ($X=\text{Cl}, \text{Br}$) have been investigated under hydrostatic pressure (0–8 GPa) using a plane wave basis set of Quantum ESPRESSO (QE). Perdew–Burke–Ernzerhof for Solids (PBESol) was used as exchange–correlation functional. The article is structured as follows: Section 2 provides the computational details, Section 3 presents the results and discussion of the results, and Section 4 contains the conclusion.

2. Computational details

The plane-wave basis set of the Quantum ESPRESSO algorithm, which is based on Density Functional Theory (DFT) [6, 7], was used to carry out the calculations. DFT is a helpful technique used in material discovery that can be utilized to investigate known as well as unknown material properties. Norm-conserving pseudopotentials (NCPP) [14] were utilized in this study to characterize the electron-ion interactions. All structural optimization and property calculations were performed between 0 and 8 GPa of external hydrostatic pressure. In the Perdew–Burke–Ernzerhof for Solids (PBESol) schemes of the generalized gradient approximation (GGA) [15, 16] employed in the study, the atomic potential was defined by means of the electron exchange–correlation energy function. For every atom, the corresponding cut-off energy, energy, and force convergence thresholds were obtained to be 120 Ry, 10^{-5} eV, and

10^{-5} eV \AA^{-1} , respectively. For structural optimization, band gap, optical properties, and mechanical properties, an a-centered $6 \times 6 \times 6$ K-mesh in the Brillouin zone was used [17], whereas K-points of $12 \times 12 \times 12$ and $32 \times 32 \times 32$ were used for the density of state (DOS) and partial density of state (PDOS) calculations, respectively. Calculations of opto-electronic, mechanical, and thermoelectric properties have also been carried out. The BFGS (Broyden-Fletcher-Goldfarb-Shanno) quasi-Newton algorithm was employed for comprehensive structural relaxation, and the atom locations were fully optimized for DOS, PDOS, and optical properties [18, 19].

2.1. Optical properties calculation

The dielectric function $\varepsilon(\omega) = \varepsilon_1(\omega) + \varepsilon_2(\omega)$, which is involved in characterizing the optical properties of materials, can be used to macroscopically define the optical response function. The imaginary component ($\varepsilon_2(\omega)$) of the dielectric function can be found using the momentum matrix elements between the occupied and unoccupied electronic states, as stated in equation (2). Equation (1) illustrates how the Kramers-Kronig relation may also be used to compute the real part ($\varepsilon_1(\omega)$) of the dielectric function. When designing optical devices for the double-perovskite materials under study, these optical constants play a crucial role.

$$\varepsilon_1(\omega) = \frac{2}{\pi} \rho \int_0^{\infty} \frac{\omega' \varepsilon_2 \omega'}{\omega'^2 - \omega^2}, \quad (1)$$

$$\varepsilon_2(\omega) = \frac{-2}{\pi} \rho \int_0^{\infty} \frac{\omega' \varepsilon_2 \omega'}{\omega'^2 - \omega^2}. \quad (2)$$

The optical properties were studied for $\text{Rb}_2\text{SeCl}_6/\text{Br}_6$ double perovskite materials under hydrostatic pressure (0-8 GPa) by utilizing the real and imaginary components of the dielectric function. The optical properties considered include the following: absorption coefficient ($I(\omega)$), electron energy-loss functions ($L(\omega)$), extinction coefficient ($K(\omega)$), optical conductivity ($\text{Re}(\sigma)$), reflectivity ($R(\omega)$), and refractive index ($n(\omega)$). The following expressions are utilized in their computation [10, 20, 21]:

$$n(\omega) = \sqrt{\frac{|\varepsilon(\omega)| + \varepsilon_1(\omega)}{2}}, \quad (3)$$

$$R(\omega) = \frac{(n-1)^2 + k^2}{(n+1)^2 + k^2}, \quad (4)$$

$$\text{Re}(\sigma) = \frac{\omega}{4\pi} \varepsilon_2(\omega), \quad (5)$$

$$K(\omega) = \sqrt{\frac{|\varepsilon(\omega)| - \varepsilon_1(\omega)}{2}}, \quad (6)$$

$$L(\omega) = \frac{\varepsilon_2}{\varepsilon_1^2 + \varepsilon_2^2}, \quad (7)$$

$$I(\omega) = \sqrt{2} \omega \left(\frac{\varepsilon_1(\omega)^2 + \varepsilon_2(\omega)^2 - \varepsilon_1(\omega)}{2} \right)^{\frac{1}{2}}. \quad (8)$$

2.2. Mechanical properties calculation

It is vital to understand a material's mechanical qualities, such as brittleness, ductility, deformation, strain, stress, and hardness, during the production process. Long-lasting and successful device applications require mechanically stable compounds. Cubic compounds meet the Born criteria [10, 20, 21]. The elastic constants C_{11} , C_{12} , and C_{44} are used in this definition. Born *et al.* [22] later looked into the Born-Huang theory [22], which was created by Max Born and Kun Huang and offers a comprehensive explanation of a material's mechanical stability. The following are the stability conditions for the cubic crystal structure [22]:

$$C_{11} - C_{12} > 0, \quad (9)$$

$$C_{11} - 2C_{12} > 0, \quad (10)$$

$$C_{44} > 0, \quad (11)$$

and

$$C_{11} < B < C_{44}. \quad (12)$$

The bulk modulus (B) in equation (12) above is calculated using:

$$B = \frac{C_{11} + 2C_{12}}{3}. \quad (13)$$

A material with a low C_{12} value compresses more easily in the C_{12} direction compared to other directions [10, 20]. Voigt [23], Reuss [24], and Hill [25] found a correlation between the elastic constant and various isotropic properties, such as bulk modulus, shear modulus, and young modulus. Chung and Buessem developed the Voigt-Reuss-Hill Approximation (VHR) [26], which incorporates this relationship. Voigt's elastic modulus equations are as follows:

$$B_V = \frac{C_{11} + 2C_{12}}{3}, \quad (14)$$

$$G_V = \frac{C_{11} - C_{12} + 3C_{44}}{5}, \quad (15)$$

B_V and G_V denote the isotropic bulk and shear moduli, respectively. For a cubic structure, Reuss' bulk modulus (B_R) and Voigt's (B_V) are comparable. Equation (16) denotes Reuss' shear modulus (G_R) [24]:

$$G_R = \frac{5(C_{11} - C_{12})C_{44}}{4C_{44} + 3(C_{11} - C_{12})}. \quad (16)$$

The Hill's elastic moduli approximation is used to get the average of Voigt's and Reuss' elastic moduli values [25].

$$B_H = \frac{1}{2}(B_V + B_R), \quad (17)$$

$$G_H = \frac{1}{2}(G_V + G_R). \quad (18)$$

Hill's bulk (G_H) and shear moduli (B_H) are computed using equations (17) and (18) [22]. The bulk modulus of a material measures its strength, while the shear modulus measures its resistance to transverse deformations about its hardness [10, 27, 28]. A greater shear modulus value shows a material's ductility and resistance to plastic deformation [10, 27]. The expressions for calculating shear anisotropy (A), Cauchy pressure (P_C), Young's modulus (Y), Poisson's ratio (ν), and Pugh's ratio (R_p) are as follows:

$$A = \frac{2C_{44}}{C_{11} - C_{12}}, \quad (19)$$

$$P_C = C_{12} - C_{44}, \quad (20)$$

$$Y = \frac{9BG}{3B + G}, \quad (21)$$

$$\nu = \frac{3B - 2G}{6B + 2G}, \quad (22)$$

$$R_p = \frac{B}{G}. \quad (23)$$

2.3. Thermoelectric properties calculation

The BoltzTraP2 package [29] was used in this work to calculate the thermoelectric characteristics (TE) of $\text{Rb}_2\text{SeCl}_6/\text{Br}_6$. The BoltzTraP2 package operates within the DFT framework written in QE code, with a relaxation time constant of 10^{-14} s. The thermoelectric properties evaluated include electronic thermal conductivity (κ_e), Seebeck coefficient (S), electrical conductivity (σ/τ), power factor (PF), and figure of merit (ZT) at temperatures ranging from 150–1300 K. The Seebeck coefficient and electronic thermal conductivity have a significant impact on the figure of merit (ZT), and these thermoelectric characteristics are reliant on the relaxation time constant. PF is calculated using the following expression [10]:

$$PF = S^2\sigma, \quad (24)$$

while the figure of merit (ZT) is calculated using:

$$ZT = \frac{\sigma S^2}{\kappa_e} T. \quad (25)$$

3. Results and discussion

3.1. Electronic Properties

To fully comprehend the photoelectric conversion efficiency (PCE) of perovskite solar cell materials, it is necessary to examine their electrical structure. The energy band structure (BS), density of states (DOS), and partial density of state (PDOS) of the investigated double perovskite materials are calculated under hydrostatic pressure (0–8 GPa).

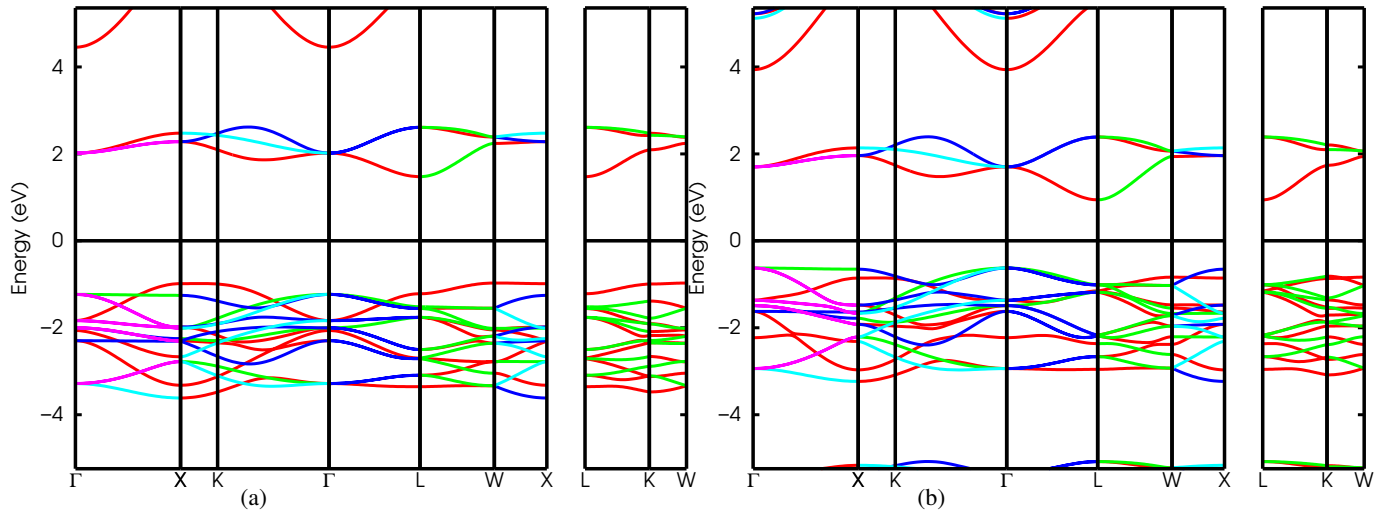


Figure 1: Band structure plots at 0 GPa for (a) Rb_2SeCl_6 and (b) Rb_2SeBr_6 .

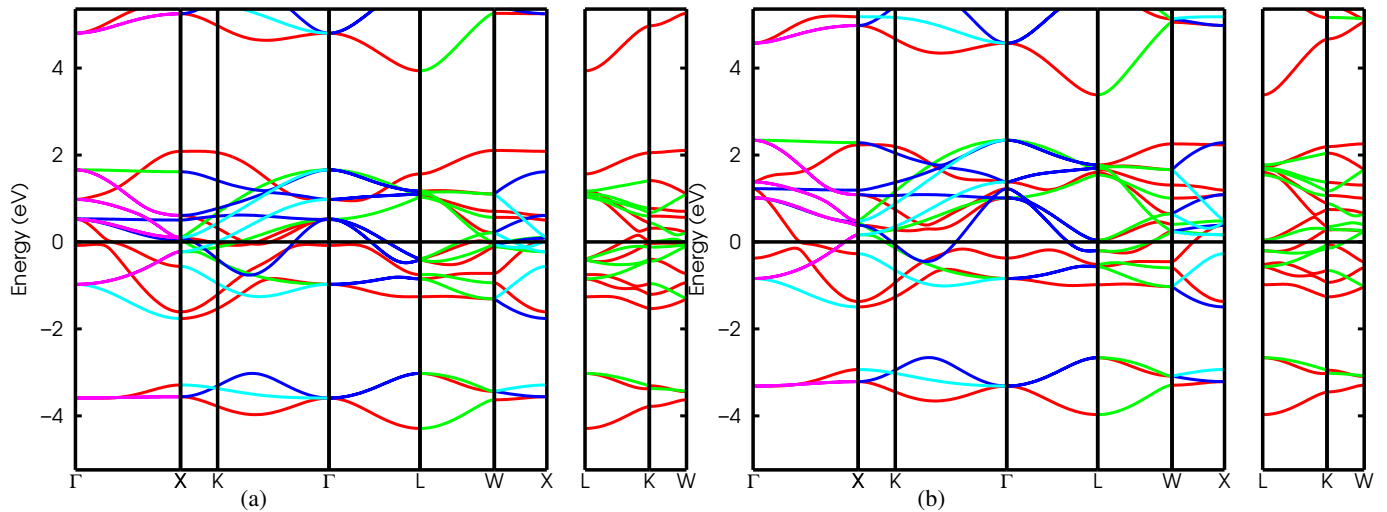


Figure 2: Band structure plots at 8 GPa for (a) Rb_2SeCl_6 and (b) Rb_2SeBr_6 .

3.1.1. Band structure

The effect of hydrostatic pressure on the band gap energy of the $\text{Rb}_2\text{SeCl}_6/\text{Br}_6$ double perovskite materials were studied. Figures 1 and 2 show the band structure of $\text{Rb}_2\text{SeCl}_6/\text{Br}_6$ under hydrostatic pressure (0–8 GPa). Band structure plots reveal dispersion along high-symmetry regions in the Brillouin Zone. Table 1 shows that at certain hydrostatic pressure levels, the examined materials exhibit metallic and indirect band gap semiconductor characteristics. This means that the studied materials' VBM (valence band maximum) and CBM (conduction band minimum) do not share the same symmetry points at some hydrostatic pressure levels, but their band gaps are suitable for opto-electronic applications. At some hydrostatic pressure values, bands are crossing the fermi energy (E_F) from VBM to CBM, as shown in Figure 2.

Table 1 shows that replacing Br atoms with Cl atoms reduces the energy band gap of Rb_2SeX_6 ($X=\text{Cl},\text{Br}$) by the order of $\text{Rb}_2\text{SeBr}_6 < \text{Rb}_2\text{SeCl}_6$. The band gap likewise decreases when hydrostatic pressure increases from 0 to 8 GPa. Table 1 shows that Rb_2SeCl_6 have band gap value 2.44 eV at 0 GPa, 2.21 eV at 2 GPa, and 0.00 eV at pressure values ≥ 4 GPa, due to bands crossing E_F from VBM to CBM.

At 0 GPa, Rb_2SeBr_6 has band gap value of 1.56 eV. At pressure value ≥ 2 GPa, Rb_2SeBr_6 has band gap values of 0.00 eV, indicating that the material has metallic nature. This shows that Rb_2SeBr_6 at 2–8 GPa hydrostatic pressure values has a metallic character as the bands cross from VBM to CBM, as seen in Figure 2. The band structure results also demonstrate that hydrostatic pressure has an effect on changing the material's semiconductor nature to metallic nature, as it converts the indirect semiconducting

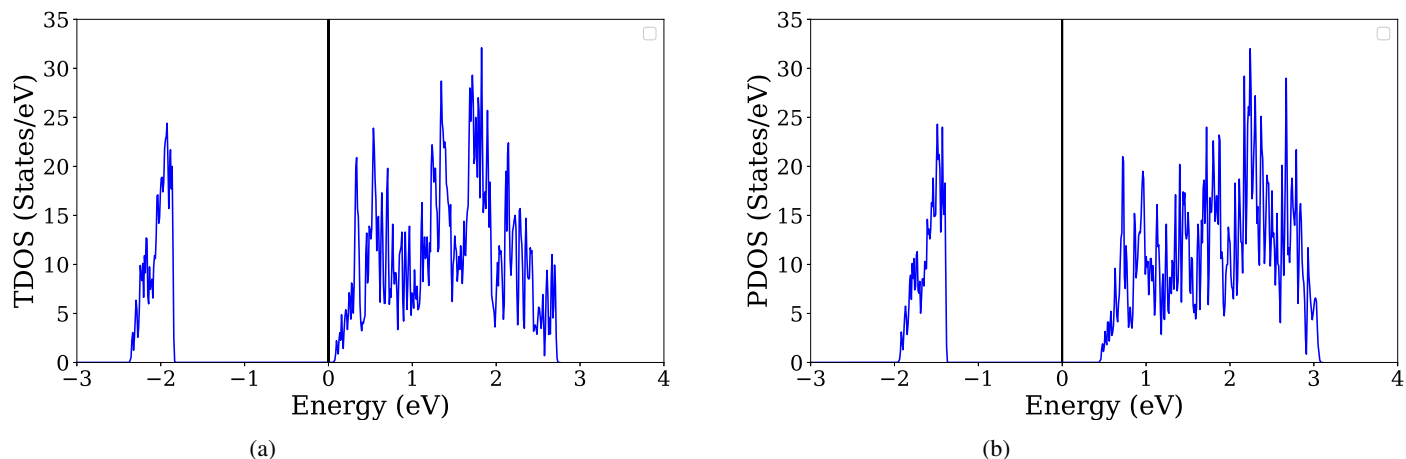


Figure 3: Density of state plots at 0 GPa for (a) Rb_2SeCl_6 and (b) Rb_2SeBr_6 .

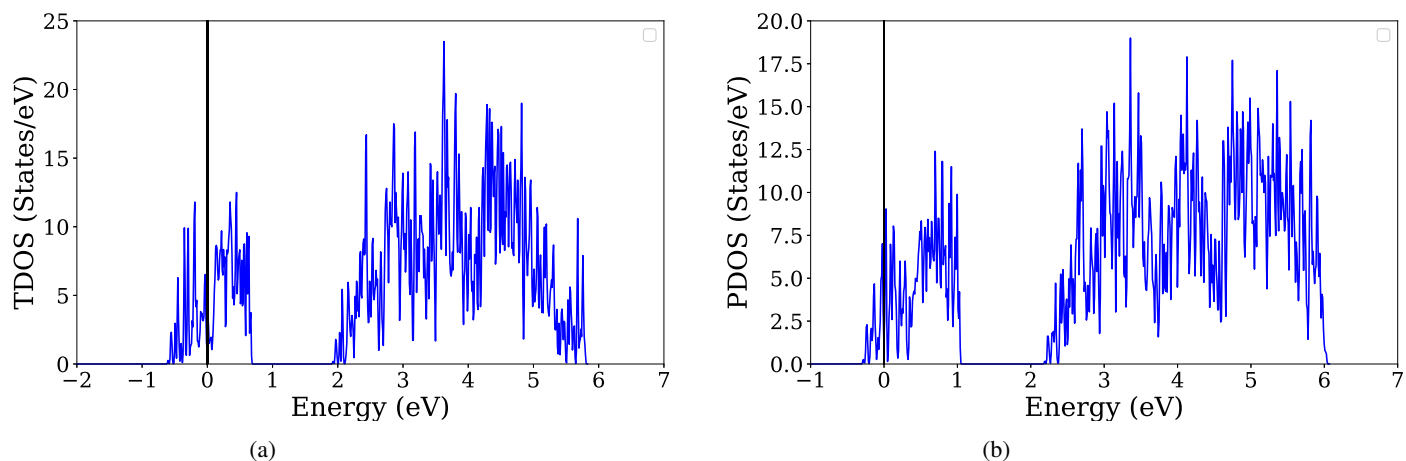


Figure 4: Density of state plots at 8 GPa for (a) Rb_2SeCl_6 and (b) Rb_2SeBr_6 .

Table 1: Calculated electronic band gap of Rb_2SeX_6 ($X=\text{Cl}, \text{Br}$) double perovskites materials under hydrostatic pressure (0-8 GPa).

Pressure (GPa)	Rb_2SeCl_6	Other Works	Rb_2SeBr_6	Other Works
0 (GPa)	2.44	2.819, 2.912 [12], 2.48, 3.20 [13]	1.56	1.755, 1.93 [12], 1.60, 2.37 [13]
2 (GPa)	2.21	-	0.00	-
4 (GPa)	0.00	-	0.00	-
6 (GPa)	0.00	-	0.00	-
8 (GPa)	0.00	-	0.00	-

nature of the studied double perovskite with higher band gap energy to low band gap energy and then to metallic nature. These compounds' band gap values demonstrate their usefulness in the design and development of photonic, electrical, and opto-electronic devices.

3.1.2. Density of state

Total density of states (TDOS) and partial density of states (PDOS) reflect a material's transport qualities. They are commonly employed to highlight the contribution of different states to band formation [3]. The TDOS and PDOS graphs in Figures 3-6

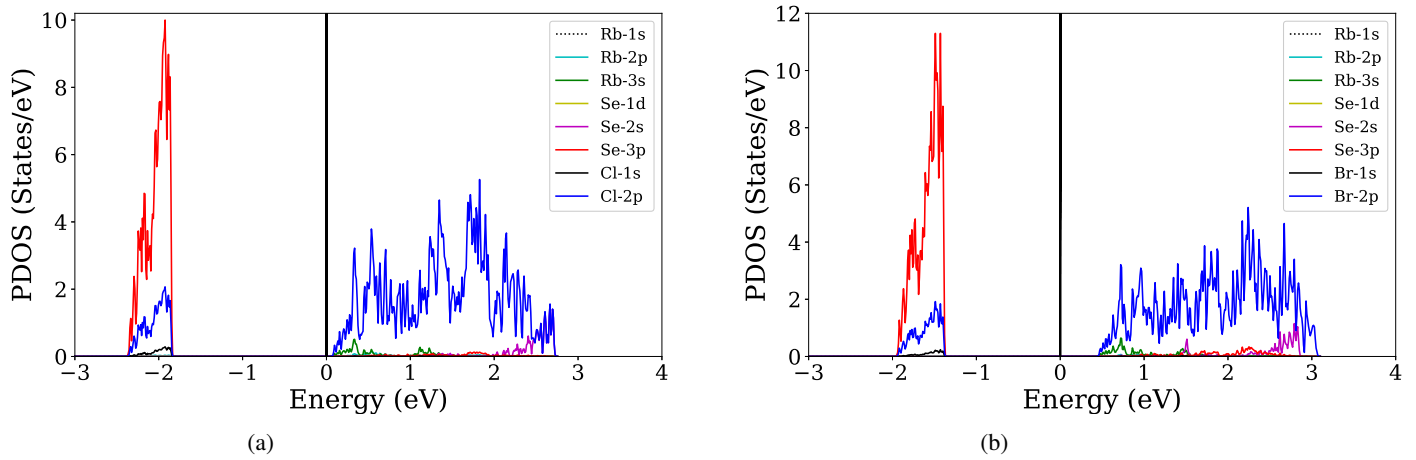


Figure 5: Partial density of state plots at 0 GPa for (a) Rb_2SeCl_6 and (b) Rb_2SeBr_6 .

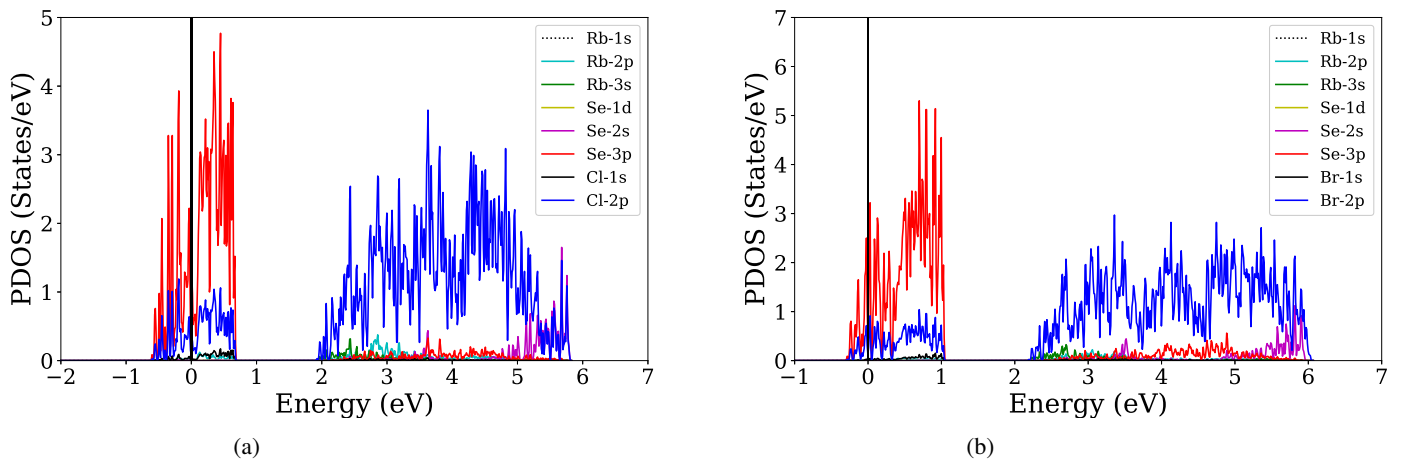


Figure 6: Partial density of state plots at 8 GPa for (a) Rb_2SeCl_6 and (b) Rb_2SeBr_6 .

demonstrate consistent band gaps and topologies. At the Fermi energy level area, electrons' contributions to each state were revealed as they moved from the valence band to the conduction band. TDOS plots show the contribution of the constituent atoms' basic atomic orbitals to the electronic state at the valence band that makes up the structure. The computed PDOS shows that the valence band at 0–4 GPa is largely composed of Se-3p and Cl-2p orbitals, whereas the conduction band is primarily composed of Cl-2p, Se-2s, and Rb-3s orbitals. The valence band shows clear hybridization between Se-3p and Cl-2p, but the conduction band shows anti-bonding hybridization between Cl-2p, Se-2s, and Rb-3s. The bands transition from VBM to CBM, causing the band gap energy to drop as the pressure changes from 0 to 8 GPa, as illustrated in the PDOS plots. Hydrostatic pressure buckles the band gap engineering of the examined double perovskite materials due to a decrease in energy band gap, causing the material's nature to change from semiconductor to metal.

3.2. Optical properties

All plots showing the computed optical properties of the $\text{Rb}_2\text{SeCl}_6/\text{Br}_6$ double perovskite materials are within the incident photon energy range of 0 to 30 eV at hydrostatic pressures of 0 to 8 GPa. Observing the variation of $\epsilon_1(\omega = 0)$ (the real part of the dielectric constant) with photon energy reveals how much the materials are polarized by the light that enters at the photonic optimum frequency. The static values ($\epsilon_1(0)$) of Rb_2SeCl_6 range from 4.7 to 6.2, as shown in Figure 7, while the static values for Rb_2SeBr_6 is between 6.3–8.6.

Figure 8 shows the plots of $\epsilon_2(\omega)$ as a function of the energy (in eV) for $\text{Rb}_2\text{SeCl}_6/\text{Br}_6$ double perovskite materials. The study found that the double perovskite materials have maximum $\epsilon_2(0)$ values between 3.5 and 4.5 eV for 0–8 GPa. The plots indicate that

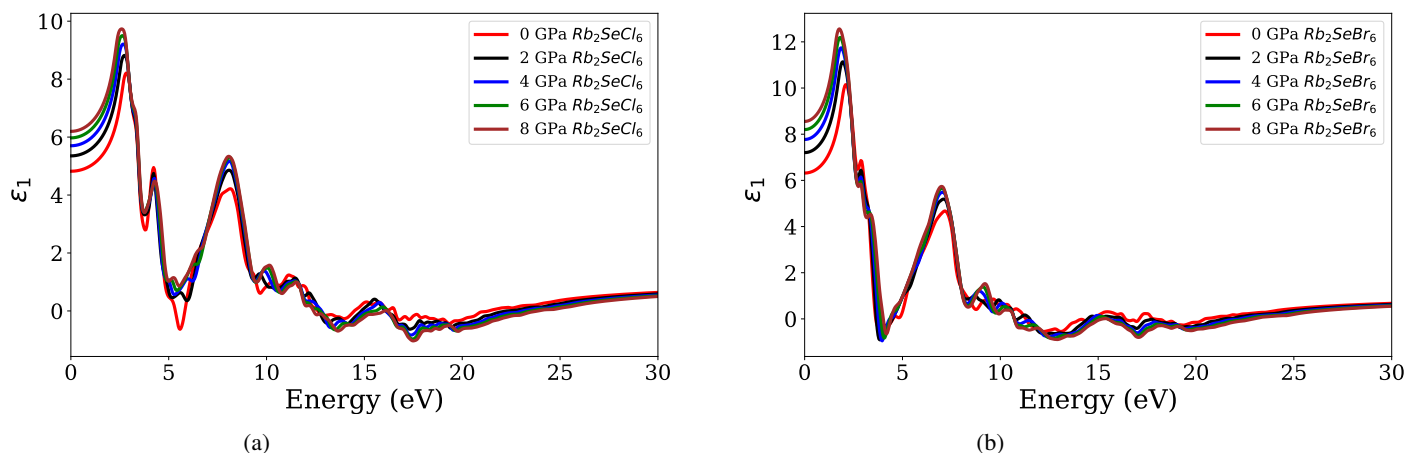


Figure 7: Real dielectric function plots for (a) Rb_2SeCl_6 and (b) Rb_2SeBr_6 .

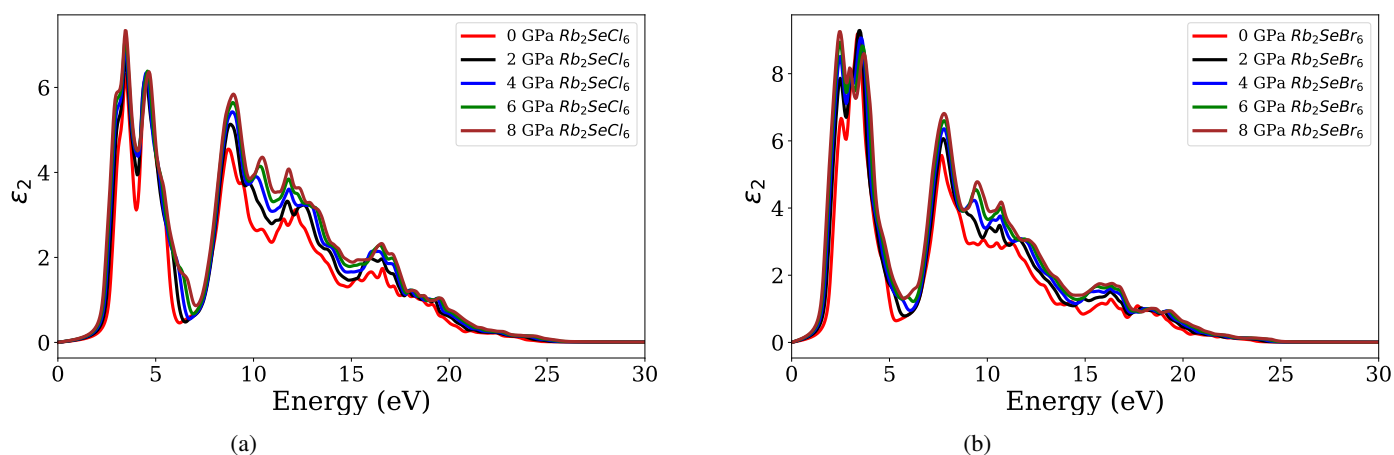


Figure 8: Imaginary dielectric function plots for (a) Rb_2SeCl_6 and (b) Rb_2SeBr_6 .

the greatest value of $\varepsilon_2(\omega)$ was obtained at 8 GPa, and the lowest value was at 0 GPa. Also Rb_2SeBr_6 has higher $\varepsilon_2(0)$ values than Rb_2SeCl_6 for all hydrostatic pressures utilized in the computation. The increased dielectric constant values of $\text{Rb}_2\text{SeCl}_6/\text{Br}_6$ double perovskite materials make them suitable for use in electrostatic capacitors such as New Paradigm Super (NPS) capacitors [30]. When developing electrical devices, greater and lower dielectric constant values are critical.

The refractive index ($n(\omega)$) describes the material's transparency and light dispersion. Figure 9 shows plots of $n(\omega)$ and photon energy at hydrostatic pressures ranging from 0–8 GPa. The refractive index, an important physical feature in optics, describes how light behaves inside materials. According to Nabi *et al.* [31], the refractive index of a substance varies with the velocity of light passing through different media. The static values $n(0)$ for all examined double perovskite materials range from 2.2 to 2.9 at all hydrostatic pressure values considered. Figure 9 indicate that the maximum values of $n(\omega)$ were discovered at hydrostatic pressure value of 8 GPa and the lowest values at 0 GPa. The static values of the refractive index is found to increase with increase in hydrostatic pressure. The Figure reveals that the explored double perovskite materials have high refractive index in the 3-4 eV photon energy range, indicating that they are more appropriate for visible area operation [32]. Since the materials refractive index values are greater than unity at all hydrostatic pressure values, this indicates the materials' transparent behavior [33].

Materials' morphology is determined by light reflection, which indicates surface roughness [10, 32]. The static values of the reflectivity ($R(0)$) is found to increase with hydrostatic pressure for the two materials, as demonstrated in Figure 10. Higher values are obtained around photon energies values of 21 and 24 eV. When compared to Rb_2SeBr_6 , Rb_2SeCl_6 shows increased reflectivity. Optical devices can employ high reflectivity materials, while anti-reflection devices can use low reflectivity materials [34].

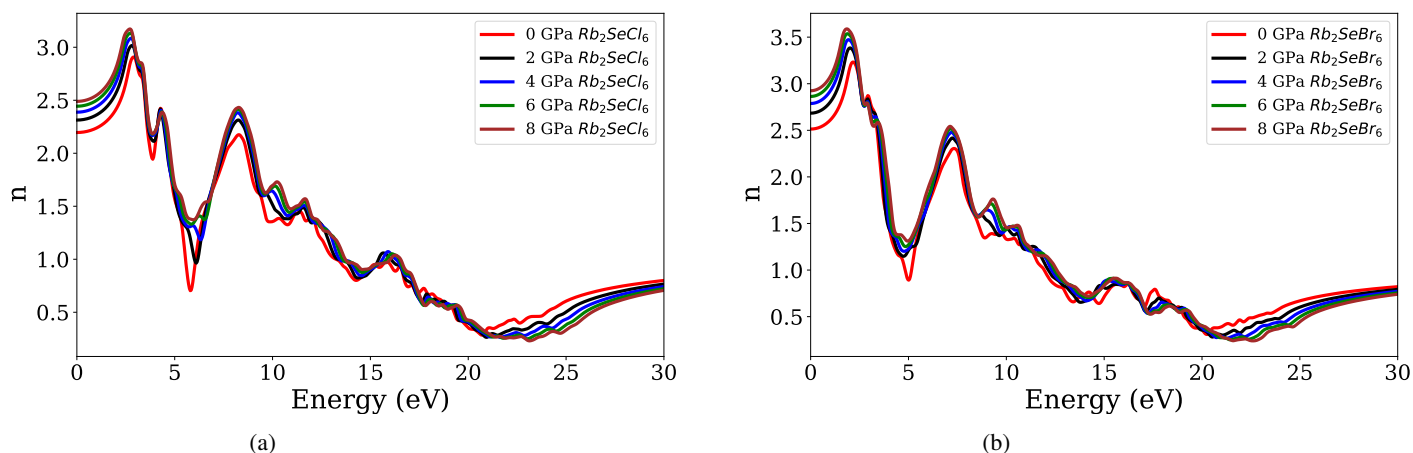


Figure 9: Refractive index plots for (a) Rb_2SeCl_6 and (b) Rb_2SeBr_6 .

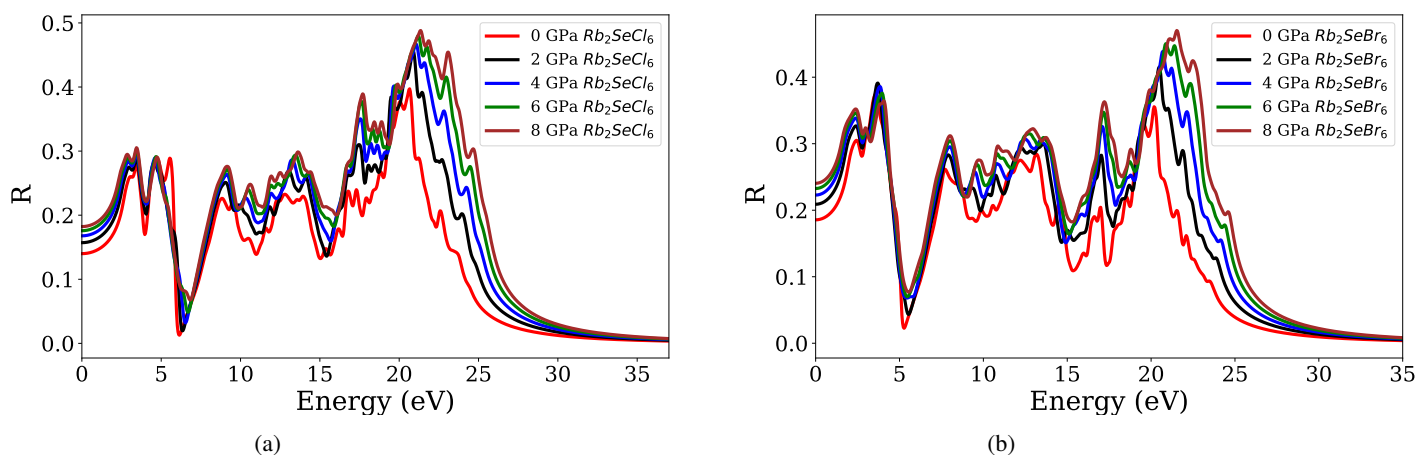


Figure 10: Reflectivity plots for (a) Rb_2SeCl_6 and (b) Rb_2SeBr_6 .

The optical conductivity ($\text{Re}(\sigma)$) demonstrates the generation of free electrons due to incoming energy absorption, with a maximum value of 7 eV. The incident energy absorption creates free carriers, resulting in an advancing current [10, 30]. Figure 11 shows the optical conductivity ($\text{Re}(\sigma)$) of $\text{Rb}_2\text{SeCl}_6/\text{Br}_6$ under hydrostatic pressure from 0 to 8 GPa, which rises with increase in pressure, like several other optical characteristics of the studied double perovskite materials. Over a certain range of photon energy (2–25 eV). The results demonstrate that at all hydrostatic pressure values, $\sigma(0)$ was about 0.20 to 0.30 for $\text{Rb}_2\text{SeCl}_6/\text{Br}_6$ in the range of photon energy 8.0 eV to 9.5 eV. In comparison to Rb_2SeCl_6 , Rb_2SeBr_6 exhibits higher optical conductivity. As a result, incident energy absorption generates free carriers that induce an advancing current. The optical conductivity calculations reveal that the two materials can be exploited in opto-electronics applications.

The electron energy loss function ($L(\omega)$) has a considerable influence on the energy loss of fast electrons traveling through the material and is typically maximum at plasma energy [10, 20]. Electron energy-loss spectroscopy [35] measures the energy distribution of electrons interacting with a specimen and losing energy due to inelastic scattering. Equation 7 was used to calculate the electron energy-loss spectrum of $\text{Rb}_2\text{SeCl}_6/\text{Br}_6$ at hydrostatic pressures ranging from 0 to 8 GPa. The EELS for Rb_2SeX_6 ($X=\text{Cl}, \text{Br}$) falls within the 21–24 eV photon energy range, as illustrated in Figure 12. Maximum EELS values were obtained at roughly 4.0–7.1. The findings also demonstrate that the peak EELS values of the examined double perovskite materials increase with increase in the hydrostatic pressure. When compared to Rb_2SeBr_6 , Rb_2SeCl_6 has higher EELS. Peaks in the reflectivity spectrum and the energy loss spectrum occur in roughly the same photon energy range. This clearly shows that infrared and visible energy ranges have lower energy losses [36]. The studied materials exhibit insignificant $L(\omega)$ values around 5 eV and very low values near 10 eV, allowing

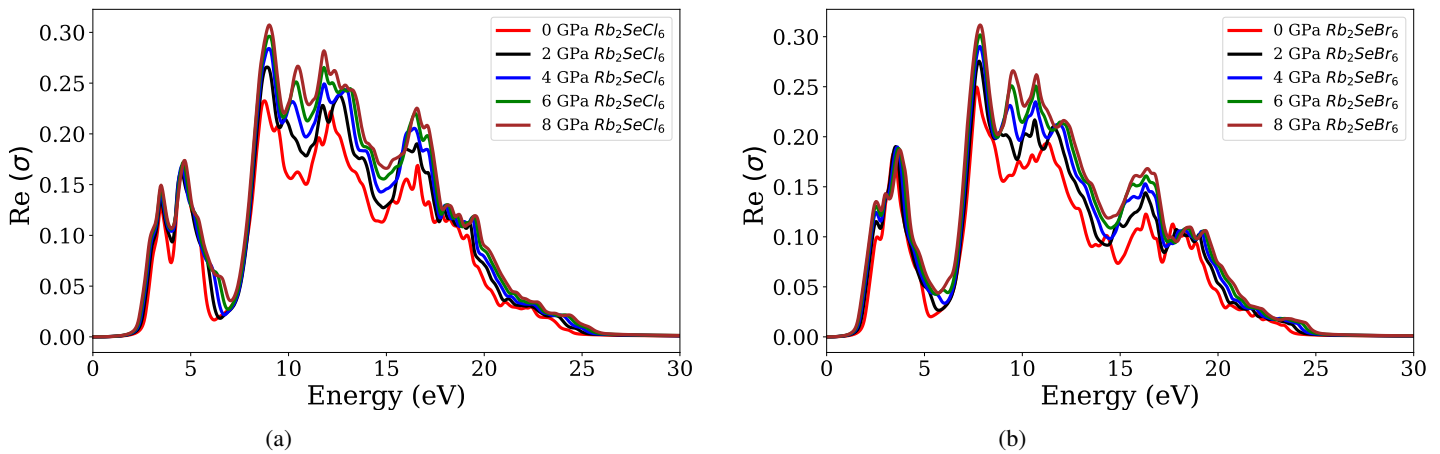


Figure 11: Optical conductivity plots for (a) Rb_2SeCl_6 and (b) Rb_2SeBr_6 .

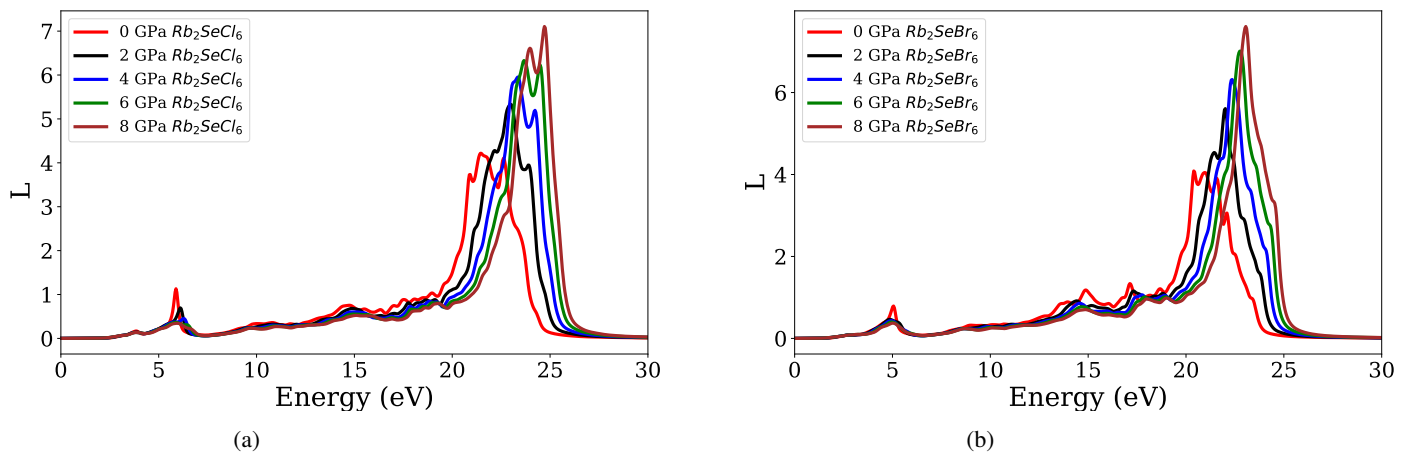


Figure 12: Electron energy loss plots for (a) Rb_2SeCl_6 and (b) Rb_2SeBr_6 .

them to be used in a wide range of opto-electronic applications in the visible and ultraviolet areas [37].

The extinction coefficient, $K(\omega)$, defines electromagnetic waves' movement through any medium [10, 31]. It is also an important physical characteristic related to a material's ability to absorb light at a specific frequency. Figure 13 shows the plots $K(\omega)$ against energy. The Figure shows that $K(\omega)$ increases with hydrostatic pressure. maximum $K(\omega)$ values were observed for all studied double perovskite materials between 3.5 and 5.0 eV. Extinction coefficients were highest at 2 GPa (2.05) and 4 GPa (2.0), and lowest at 6 GPa (1.90) and 8 GPa (1.65), as depicted in the plot.

Semiconductor optical properties are crucial for modeling quantum structures [38]. The absorption coefficient ($I(\omega)$) is a physical metric that represents the distance that incident light of a specific wavelength travels through a material before being absorbed [38]. According to Ref. [39], the absorption coefficient ($I(\omega)$) measures the attenuation of light energy per centimeter in a material. Figure 14 shows the computed values of $I(\omega)$ for $\text{Rb}_2\text{SeCl}_6/\text{Br}_6$ under hydrostatic pressures. The maximum value of the absorption coefficient increases with hydrostatic pressure, reaching higher values at photon energies of 17–18.5 eV. The Figure also shows that Rb_2SeCl_6 has higher $I(\omega)$ values than Rb_2SeBr_6 . A high value of $I(\omega)$ allows the use of the material for optical properties applications.

Hydrostatic pressure has a significant impact on the optical behavior of the examined double perovskite materials because it increases their optical characteristics. The optical properties of $\text{Rb}_2\text{SeCl}_6/\text{Br}_6$ confirm maximum absorption, high reflectivity, low optical loss in visible and ultraviolet regions, good optical conductivity, and a refractive index appropriate for visible range operation. As a result, the investigated double perovskite materials have become increasingly important for solar cells and other photonic applications.

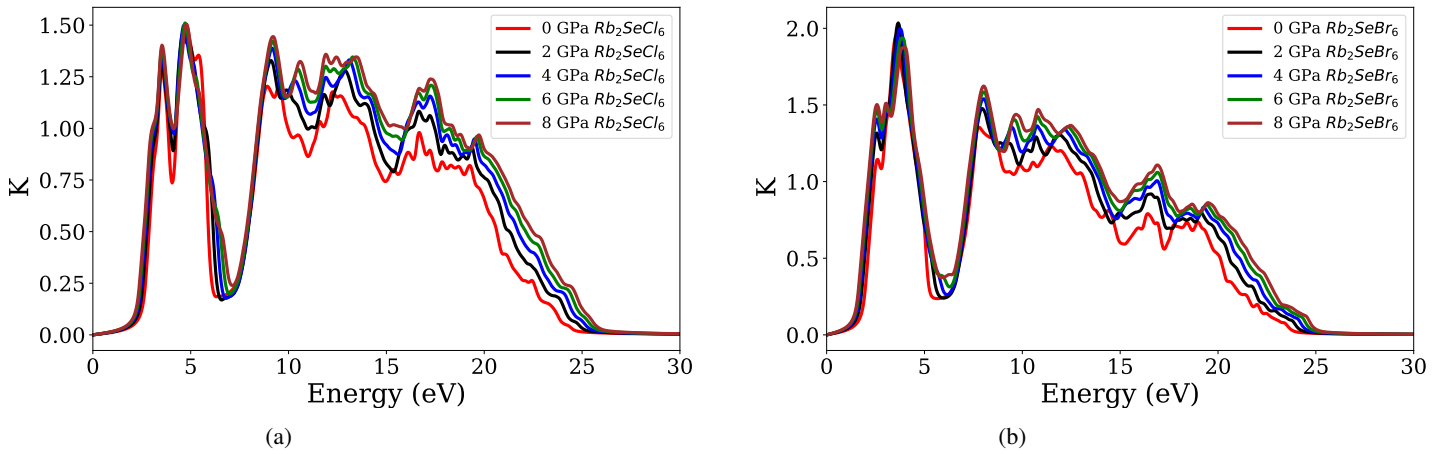


Figure 13: Extinction coefficient plots for (a) Rb_2SeCl_6 and (b) Rb_2SeBr_6 .

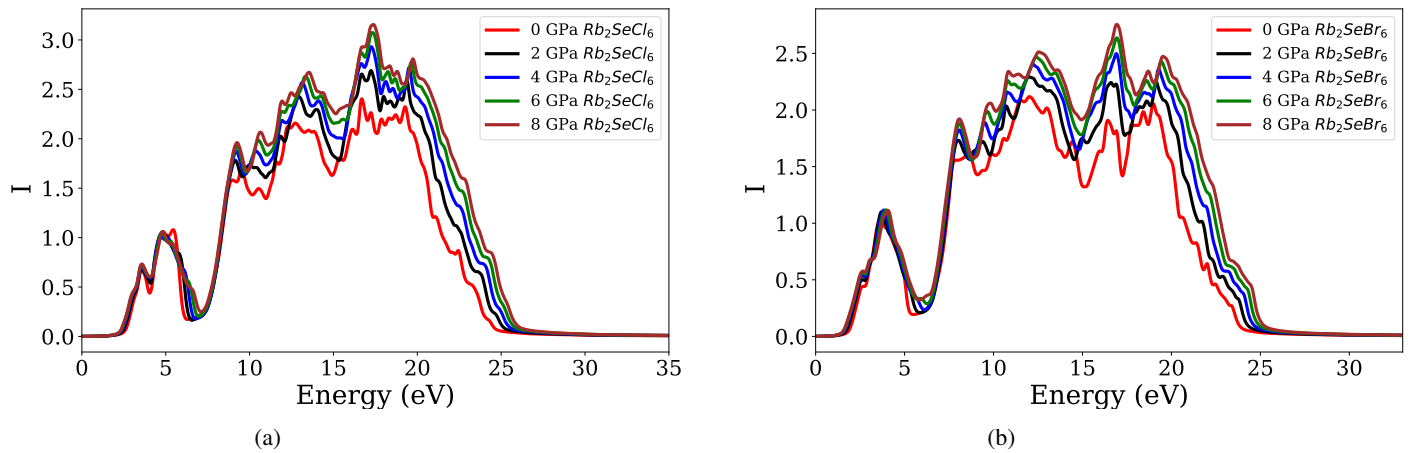


Figure 14: Absorption coefficient plots for (a) Rb_2SeCl_6 and (b) Rb_2SeBr_6 .

3.3. Mechanical properties

The elastic constants provide the basis for determining many mechanical parameters, including Young's modulus (Y), bulk modulus (B), shear modulus (G), Poisson's ratio (ν), Pugh's ratio (R_p), and shear anisotropy (A). Additionally, these mechanical characteristics can be estimated using the Voigt-Reuss-Hill approximations, particularly for polycrystalline crystals [22, 25]. Compound stability and stiffness can be characterized by describing the nature of forces acting within solids [40]. Mechanical stability criteria are computed using the required and sufficient Born criteria, especially for cubic crystal formations, stated using equations (9)-(12).

Table 2 displays the mechanical properties of $\text{Rb}_2\text{SeCl}_6/\text{Br}_6$ double perovskite materials studied at hydrostatic pressure (0 to 8 GPa). The table shows that the bulk modulus (B), C_{11} , C_{12} , and C_{44} values for $\text{Rb}_2\text{SeCl}_6/\text{Br}_6$ double perovskite materials meet the Born criteria and ensure mechanical stability at all hydrostatic pressure values (0–8 GPa). The findings show that pressure has a considerable effect on the mechanical properties of the materials under investigation. Table 2 demonstrates that the material is easily compressible in the C_{44} direction (under hydrostatic pressure), as C_{44} has the smallest value when the elastic constants are compared.

Table 2 also shows that the B , Y , and G values of $\text{Rb}_2\text{SeCl}_6/\text{Br}_6$ double perovskite materials increase with increase in hydrostatic pressure. Hydrostatic pressure increases the examined material's core forces, covalent bonding strength, and plastic deformation to resistance. A material's degree of isotropy can be calculated using its shear anisotropy (A) factor. If the material's shear anisotropy is equal to one, it is isotropic and evenly deformable along all directions of the material's body. Elastic anisotropy occurs when the

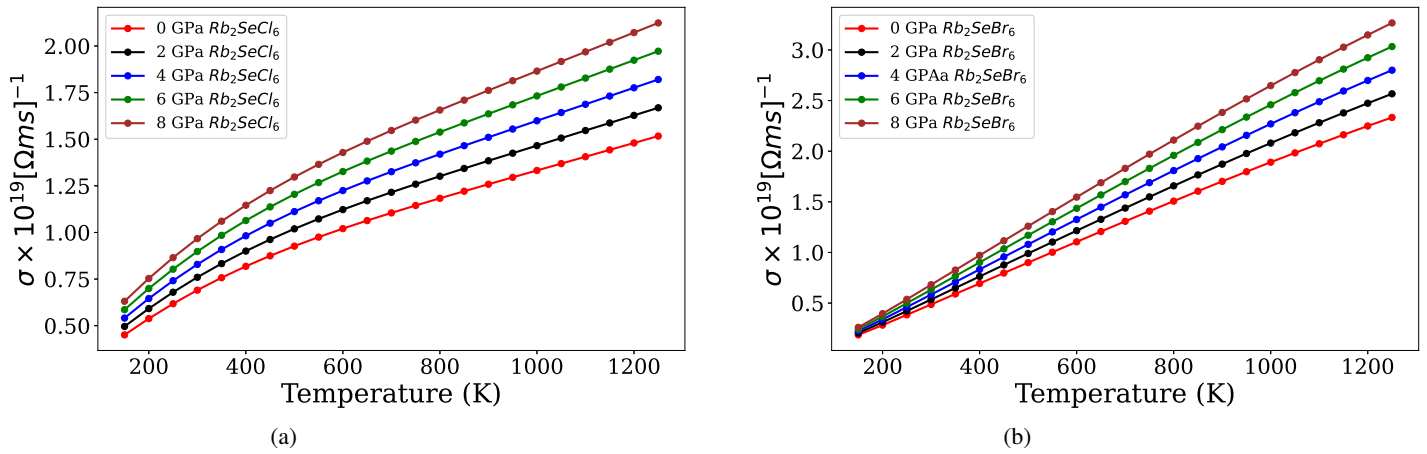


Figure 15: Plots of electrical conductivity for (a) Rb_2SeCl_6 and (b) Rb_2SeBr_6 .

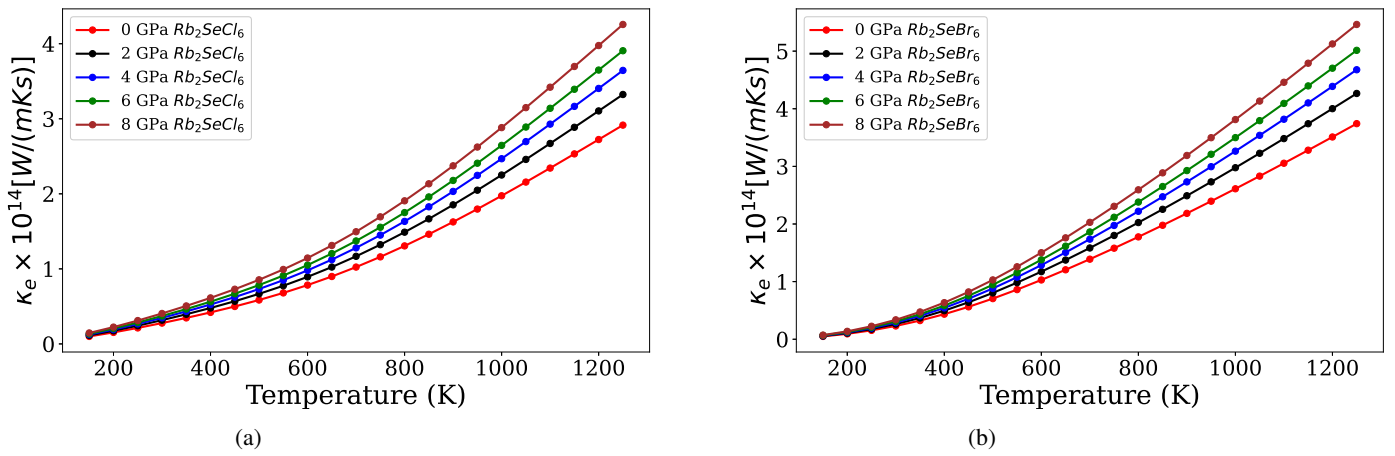
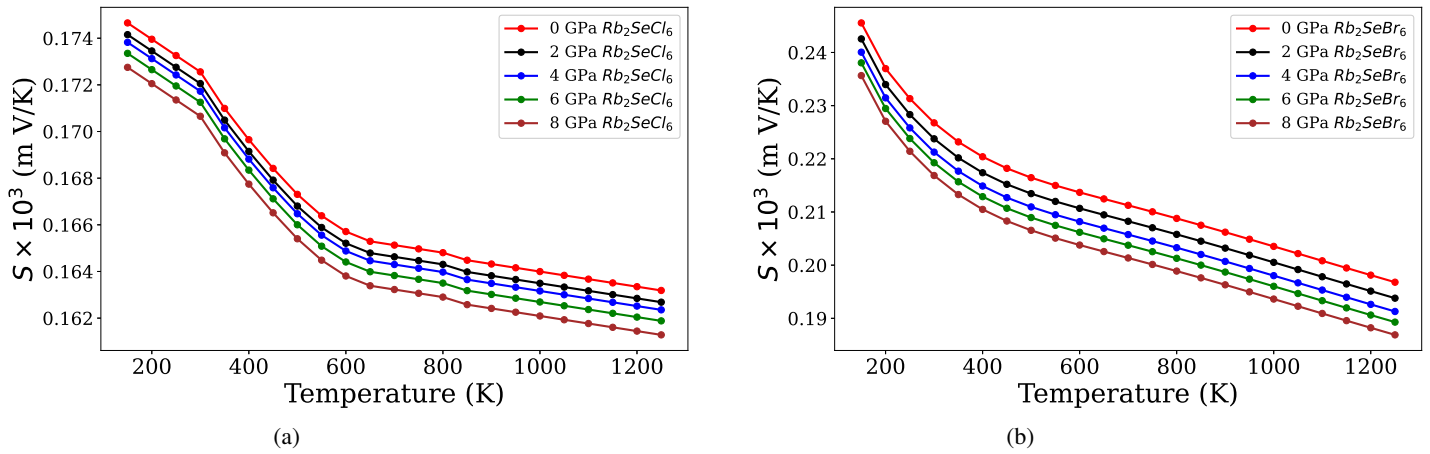
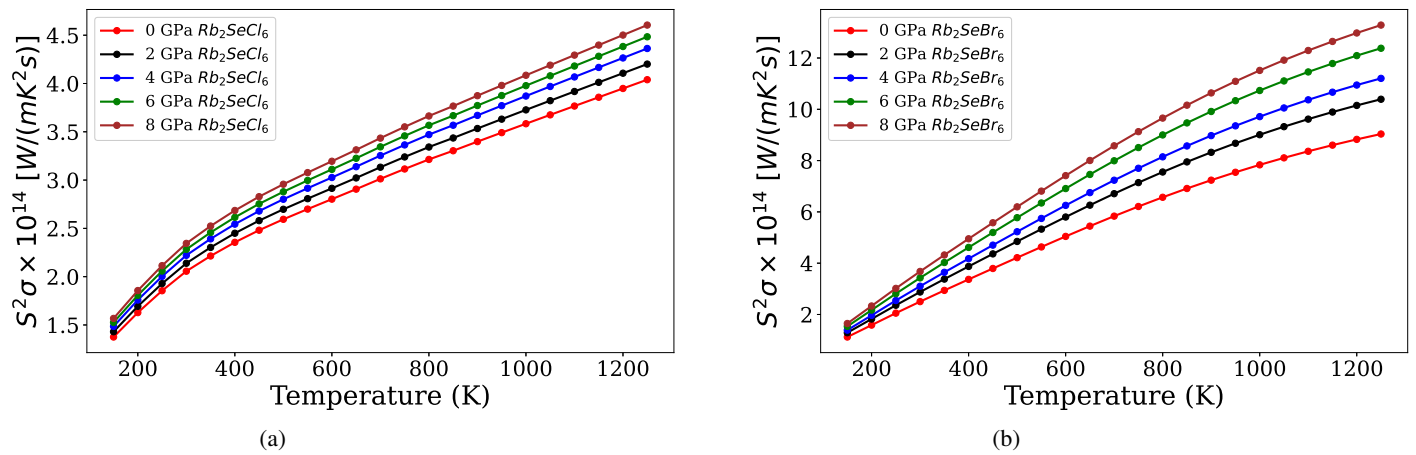


Figure 16: Plots of Thermal conductivity for (a) Rb_2SeCl_6 and (b) Rb_2SeBr_6 .

Table 2: Mechanical properties of Rb_2SeX_6 ($X=Cl, Br$) double perovskites materials under hydrostatic pressure (0-8 GPa).

Material	Pressure (GPa)	C_{11} (GPa)	C_{12} (GPa)	C_{44} (GPa)	P_C (GPa)	B (GPa)	G (GPa)	A	Y	ν	R_P
Rb_2SeCl_6	0	21.19	9.01	9.74	-0.74	23.06	7.73	1.59	19.38	0.25	1.68
	2	38.05	19.99	16.25	3.73	26.01	12.84	1.79	33.07	0.28	2.02
	4	52.15	30.99	22.76	8.22	37.13	17.48	2.15	43.78	0.29	2.12
	6	66.45	39.76	29.59	10.16	49.86	21.11	2.21	53.39	0.30	2.36
	8	79.47	47.93	32.78	15.14	58.44	24.43	2.47	64.31	0.31	2.39
Rb_2SeBr_6	0	20.22	9.60	9.13	0.47	13.14	7.34	1.71	18.57	0.26	1.78
	2	37.30	21.40	16.03	5.37	26.70	12.09	2.01	31.51	0.30	2.20
	4	51.95	31.36	21.89	9.46	38.22	16.17	2.12	42.49	0.31	2.36
	6	65.09	40.43	26.68	13.75	48.65	19.57	2.16	51.75	0.32	2.48
	8	77.35	48.04	30.29	17.11	57.81	22.91	2.11	60.70	0.32	2.52

Figure 17: Plots of Seebeck coefficient for (a) Rb_2SeCl_6 and (b) Rb_2SeBr_6 .Figure 18: Plots of Power factor for (a) Rb_2SeCl_6 and (b) Rb_2SeBr_6 .

shear anisotropy is less than or greater than one [10, 20, 21, 41, 42]. The anisotropy values of $\text{Rb}_2\text{SeCl}_6/\text{Br}_6$ double perovskite are greater than one for all hydrostatic pressures (0–8 GPa), indicating that they are elastic anisotropy materials.

The estimated Cauchy pressure (P_C) not only describes a material's ductility but also the angular nature of compounds and their metal atomic bonding [43]. Positive Cauchy pressure indicates metallic bonding and its ductility, whereas angular-directed bonding is brittle [43]. Table 2 shows that the computed P_C of $\text{Rb}_2\text{SeCl}_6/\text{Br}_6$ double perovskite materials increases with increasing hydrostatic pressure. The examined double perovskite materials have positive P_C values. This demonstrates the metallic bonding of the materials, as well as ductility. However, Rb_2SeCl_6 evaluated under 0 GPa hydrostatic pressure has negative P_C values (-0.74 GPa), indicating angular directed bonding and brittleness for the material at 0 GPa [43]. The Poisson's ratio (ν) for polycrystalline aggregate, which measures lateral deformation in a material [42], was computed using equation (22). To determine a material's brittleness and ductility, Poisson's ratio can be applied. The term "ductile" refers to a material with a ν greater than 0.26, in contrast to "brittle" [10, 33, 41]. When pressure is applied, the two materials have ν values greater than 0.26, suggesting that they are ductile. Pugh's ratio (R_P) refers to the bulk-shear modulus ratio [44]. Ductile materials have a Pugh's ratio greater than 1.75, while brittle materials have a Pugh's ratio less than 1.75 [10, 21, 41, 44]. Under hydrostatic pressure, the two materials have R_P values greater than 1.75, supporting the ductile nature of the materials under pressure.

3.4. Thermoelectric properties

The Boltztrap2 code was used in the calculations of the thermoelectric properties. The code maintains a constant relaxation time (τ) of 10^{-14} s [29]. The examination of the thermoelectric properties of $\text{Rb}_2\text{SeCl}_6/\text{Br}_6$ under hydrostatic pressure (0–8 GPa) considers

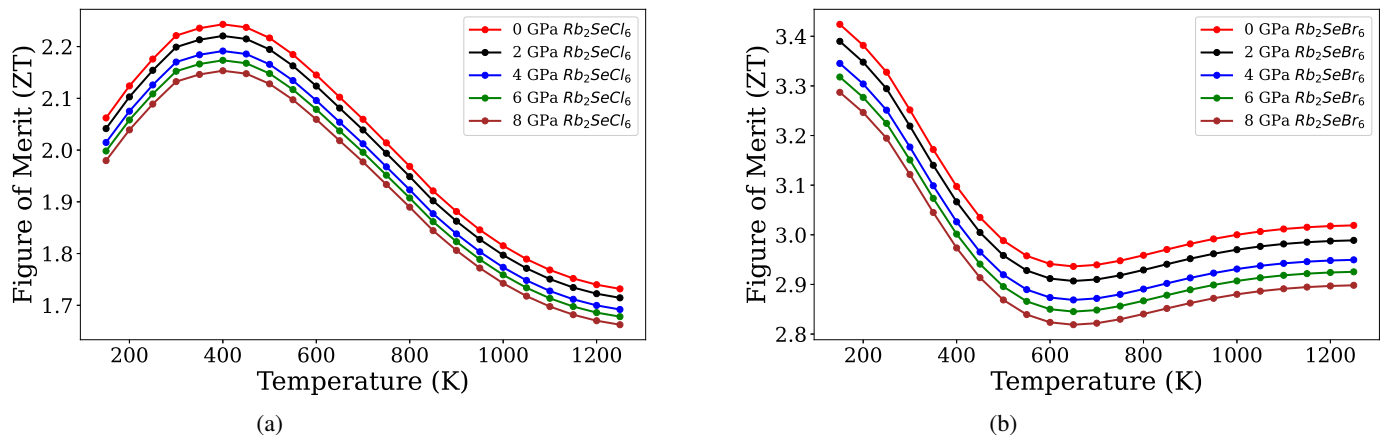


Figure 19: Plots of figure of merit for (a) Rb_2SeCl_6 and (b) Rb_2SeBr_6 .

electrical and thermal conductivities, Seebeck coefficient, power factor, and figure of merit.

Charge carrier mobility and density determine a material's electrical conductivity (σ) [8, 9]. The electrical conductivity of $\text{Rb}_2\text{SeCl}_6/\text{Br}_6$ was studied at hydrostatic pressure values of 0–8 GPa. Figure 15 depicts σ/τ plots for the examined double perovskite materials under hydrostatic pressure. Thermal conductivity (σ) was shown against a temperature range of 150–1300 K. One can see that σ rises with increasing hydrostatic pressure. Rb_2SeBr_6 has higher values of σ than Rb_2SeCl_6 at high temperatures, suggesting that it has better electrical conductivity for use as a thermoelectric material.

Thermal conductivity (κ_e) consists of two components: the lattice and the electronic thermal component, which includes the impact of electrons and holes within the material. The mathematical formula $\kappa = \kappa_e + \kappa_l$ [8–10] can be utilized to demonstrate this claim. Figure 16 depicts plots of κ_e for Rb_2SeX_6 ($X=\text{Cl}, \text{Br}$) under hydrostatic pressure and how they increase with temperature (in the range 150–1300 K). It can be observed that the values of κ_e increase with the hydrostatic pressure. κ_e has low values at 0 GPa and high values at 8 GPa. The findings also demonstrate that Rb_2SeCl_6 has lower κ_e values than Rb_2SeBr_6 . Rb_2SeCl_6 exhibits lower thermoelectric values than Rb_2SeBr_6 . The Seebeck coefficient is the ratio of voltage to temperature ($S = V/T$) [8, 10]. Seebeck coefficients (S) can be positive or negative, depending on the materials under study. When holes are the primary charge carriers in a substance, S is positive; when electrons are the predominant charge carriers, S is negative. Figure 17 shows plots of S versus temperature at different hydrostatic pressure. Rb_2SeBr_6 has greater values of S than Rb_2SeCl_6 . The positive Seebeck coefficients indicate that the main charge carriers of $\text{Rb}_2\text{SeCl}_6/\text{Br}_6$ are holes. The results also show that Rb_2SeBr_6 is a better thermoelectric material than Rb_2SeCl_6 .

The power factor (PF) is a crucial factor to consider when determining a material's suitability for thermoelectric applications. It is defined as the product of the Seebeck coefficient and electrical conductivity, as given in equation (24) [10, 11]. Figure 18 depict PF plots against temperature (150–1300 K range). As shown in the figure, PF values increase as both temperature and hydrostatic pressure rise. Rb_2SeBr_6 has greater values of PF than Rb_2SeCl_6 . The highest value of PF was found for Rb_2SeBr_6 , which is around $13 \times 10^{14} \text{ W}/(\text{mK}^2\text{S})$, while the lowest was obtained for Rb_2SeCl_6 , which is around $6.1 \times 10^{14} \text{ W}/(\text{mK}^2\text{S})$. The results also showed that Rb_2SeBr_6 has better PF values for thermoelectric applications than Rb_2SeCl_6 .

The figure of merit (ZT) demonstrates the superior caliber of thermal compounds. Low heat conductivity and electrical properties are the two most essential parameters for assessing increased thermoelectric efficiency. Materials with $ZT \geq 1$ are effective thermoelectric materials and are suitable for device engineering [10, 45]. The figure of merit ZT of $\text{Rb}_2\text{SeCl}_6/\text{Br}_6$ falls with increasing temperature, as demonstrated in Figure 19. However, all the values are ≥ 1 for the two materials (Rb_2SeBr_6 and Rb_2SeCl_6), indicating that they have good ZT values for thermoelectric device engineering.

4. Conclusion

This study examined the opto-electronic, elastic, and thermoelectric properties of Rb_2SeX_6 ($X=\text{Cl}, \text{Br}$) under hydrostatic pressure (0–8 GPa), utilizing a plane wave basis set of Quantum ESPRESSO (QE) codes. The band gap values of the materials were found to decrease when hydrostatic pressure was applied on the materials. Rb_2SeCl_6 has a band gap value of 2.44 eV at 0 GPa, 2.21 eV at 2 GPa, and has metallic nature at pressure values above 2 GPa. Rb_2SeBr_6 has a band gap value of 1.56 eV at 0 GPa, but has a metallic nature under hydrostatic pressure (2 GPa to 8 GPa). The optical properties calculations suggest that the materials have good absorption and reflectivity, little optical loss in visible and ultraviolet regions, good optical conductivity, and a refractive

index adequate for visible range operation. As a result, the investigated double perovskite materials are important for solar cells and other opto-electronic applications. The materials' bulk modulus (B), C_{11} , C_{12} , and C_{44} values all match the Born criteria, ensuring mechanical stability at all hydrostatic pressures investigated. They exhibit elastic anisotropy, as evidenced by shear anisotropy values which are larger than one at all hydrostatic pressure values. Electrical conductivity, thermal conductivity, Seebeck coefficients, and power factor all increase with increasing pressure values. Rb_2SeBr_6 has a greater value of S (0.248×10^3 (m V/k) than Rb_2SeCl_6 ($S = 0.175 \times 10^3$ (m V/k)). The positive Seebeck coefficients indicate that the main charge carriers of the materials are holes. Rb_2SeBr_6 has a higher value of PF (about 13×10^{14} W/(mK^2S)) than Rb_2SeCl_6 (about 6.1×10^{14} W/(mK^2S)). The results of ZT in this study are more than unity, indicating that the materials have good ZT values for thermoelectric device engineering. The thermoelectric results indicate that Rb_2SeBr_6 is a more effective thermoelectric material than Rb_2SeCl_6 . We conclude that hydrostatic pressure has a substantial effect on tuning the optical and thermoelectric behavior of the double perovskite materials, as increasing hydrostatic pressure causes an increase in the optical and thermoelectric parameters of the studied double perovskites.

Acknowledgment

The authors would like to thank the Department of Physics and Materials Science, Kwara State University, Malete, for providing the computational resources used in some part of this study.

References

- [1] A. Jaffe, Y. Lin & H. I. Karunadasa, "Halide perovskites under pressure: Accessing new properties through lattice compression", *ACS Energy Lett.* **2** (2017) 1549. <https://doi.org/10.1021/acseenergylett.7b00284>.
- [2] G. Liu, L. Kong, J. Gong, W. Yang, H. K. Mao, Q. Hu, Z. Liu, R. D. Schaller, D. Zhang & T. Xu, "Pressure-induced bandgap optimization in lead-based perovskites with prolonged carrier lifetime and ambient retainability", *Adv. Funct. Mater.* **27** (2017) 1604208. <https://doi.org/10.1002/adfm.201604208>.
- [3] M. Tariq, M. A. Ali, A. Laref & G. Murtaza, "Anion replacement effect on the physical properties of metal halide double perovskite $\text{Cs}_2\text{AdInX}_6$ (X=F,Cl,Br,I)", *Solid state communications* **7** (2020) 113929. <https://doi.org/10.1016/j.ssc.2020.113929>.
- [4] S. Ahmad, J. Ur-Rehman, M. Usman, S. M. Ali & M. Ali, "First-principles calculations to investigate effect of pressure on physical properties of LiNbO_3 perovskite for photocatalytic application", *Computational and Theoretical Chemistry* **1230** (2023) 114354. ISSN 2210-271X. <https://doi.org/10.1016/j.comptc.2023.114354>.
- [5] N. Rahmani, A. Shabani & J. Adam, "A theoretical study of new polar and magnetic double perovskites for photovoltaic applications", *RSC Adv.* **12** (2022) 1. <https://doi.org/10.1039/d2ra06478b>.
- [6] P. Giannozzi, S. Baroni, N. Bonini, M. Calandra, R. Car, C. Cavazzoni, D. Ceresoli, G. L. Chiarotti, M. Cococcioni, I. Dabo, A. Dal-Corso, S. de Gironcoli, S. Fabris, G. Fratesi, R. Gebauer, U. Gerstmann, C. Gougoussis, A. Kokalj, M. Lazzeri, L. Martin-Samos, N. Marzari, F. Mauri, M. Mazzarello, S. Paolini, A. Pasquarello, L. Paulatto, C. Sbraccia, S. Scandolo, G. Sclauzero, A. P. Seitsonen, A. Smogunov & P. Umari, "Quantum espresso: a modular and open-source software project for quantum simulations of materials", *J. Phys.: Condens. Matter* **21** (2009) 395502. <https://doi.org/10.1088/0953-8984/21/39/395502>.
- [7] P. Giannozzi, O. Andreussi, T. Brumme, O. Bunau, M. Buongiorno, Nardelli, M. Calandra, R. Car, C. Cavazzoni, D. Ceresoli, M. N. C. Cococcioni, I. Carnimeo, A. Dal-Corso, S. de Gironcoli, P. Delugas, J. R. A. DiStasio, A. Ferretti, A. Floris, G. Fratesi, G. Fugallo, R. Gebauer, U Gerstmann, F. Giustino, T. Gorni, J. Jia, M. Kawamura, H. Y. Ko, F. A. Kokalj, E. Küçükbenli, M. Lazzeri, M. Marsili, N. Marzari, F. Mauri, N. L. Nguyen, H. V. Nguyen, A. Otero-de-la Roza, L. Paulatto, S. Ponce, D. Rocca, R. Sabatini, B. Santra, M. Schlip, A. P. Seitsonen, A. Smogunov, I. Timrov, T. Thonhauser, P. Umari, N. Vast, X. Wu & S. Baroni, "Advanced capabilities for materials modelling with quantum espresso", *J. Phys.: Condens. Matter* **29** (2017) 465901. <https://doi.org/10.1088/1361-648X/aa8f79>.
- [8] H. H. Hegazy, M. Manzoor, W. M. Iqbal, M. Zanib, A. Dahsan & I. Kabil, "Systematically study of optoelectronics and transport properties of chalcopyrite HgAl_2X_4 (X=S,Se) compounds for solar cell device applications", *Journal of materials research and technology* **19** (2022) 1690. <https://doi.org/10.1016/j.mrt.2022.05.115>.
- [9] H. H. Hegazy, G. M. Mustafa, A. Nawaz, N. A. Noor, A. Dahshan & I. Boukhris, "Tuning of direct bandgap of $\text{Rb}_2\text{ScTiX}_6$ (X=Cl,Br,I) double perovskites through halide ion substitution for solar cell devices", *Journal of materials research and technology* **19** (2022) 1271. <https://doi.org/10.1016/j.jmrt.2022.05.082>.
- [10] W. A. Yahya, A. A. Yahaya, A. A. Adewale, A. A. Sholagberu & N. K. Olasunkanmi, "A DFT study of optoelectronic, elastic and thermoelectric properties of the double perovskites Rb_2SeX_6 (X=Br,Cl)", *J. Nig. Soc. Phys. Sci.* **5** (2023) 1418. <https://doi.org/10.46481/jnsps.2023.1418>.
- [11] S. A. Dar, R. Sharma, V. Srivastava & U. K. Sakalle, "Investigation on the electronic structure, optical, elastic, mechanical, thermodynamic and thermoelectric properties of wide band gap semiconductor double perovskite $\text{Ba}_2\text{InTaO}_6$ ", *RSC Adv.* **9** (2019) 9522. <https://doi.org/10.1039/c9ra00313d>.
- [12] X. Diao, Y. Diao, Y. Tang, G. Zhao, Y. Gu, Q. Xie, Y. Shi, L. Zhang & P. Zhu, "High-throughput screening of stable and efficient double inorganic halide perovskite materials by DFT", *Scientific Reports* **12** (2022) 2045. <https://doi.org/10.1038/s41598-022-16221-3>.
- [13] J. Li, L. Sun, X. Cao & J. Chang, "First-principles predictions of structural, mechanical and optoelectronic properties of Se-based double perovskite A_2SeX_6 (A=Rb,K;X=Cl,Br,I)", *Phys. Chem. C.* **127** (2023) 10332. <https://doi.org/10.1021/acs.jpcc.3c01097>.
- [14] D. R. Hamann, M. Schlüter & C. Chiang, "Norm-conserving pseudopotentials", *Phys. Rev. Lett.* **43** (1979) 1. <https://doi.org/10.1103/PhysRevLett.43.1494>.
- [15] J. P. Perdew, K. Burke & M. Ernzerhof, "Atoms, molecules, solids, and surfaces: applications of the generalized gradient approximation for exchange and correlation", *Phys. Rev. B* **46** (1992) 6671. <https://doi.org/10.1103/physRevB.46.6671>.
- [16] J. P. Perdew, K. Burke & M. Ernzerhof, "Generalized gradient approximation made simple", *Phys. Rev. Lett.* **77** (1996) 3865. <https://doi.org/10.1103/PhysRevLett.77.3865>.
- [17] J. D. Pack & H. J. Monkhorst "Special points for brillouin-zone integrations-a reply", *Phys. Rev. B. Condens Matter Physics* **16** (1977) 1748. <https://doi.org/10.1103/PhysRevB.16.1748>.
- [18] C. G. Broyden, "The convergence of a class of double-rank minimization algorithms 1. general considerations", *IMA J. Appl. Math. (Institute Math. Its Appl.)* **6** (1970) 76. <https://doi.org/10.1093/imamat/6.1.76>.
- [19] C. G. Broyden, "The convergence of a class of double-rank minimization algorithms: 2. the new algorithm", *IMA J. Appl. Math. (Institute Math. Its Appl.)* **6** (1970) 222. <https://doi.org/10.1093/imamat/6.3.222>.
- [20] A. A. Sholagberu, W. A. Yahya & A. A. Adewale, "Pressure effects on the opto-electronic and mechanical properties of the double perovskite $\text{Cs}_2\text{AgInCl}_6$ ", *Phys. Scr.* **97** (2022) 085824. <https://doi.org/10.1088/1402-4896/ac831d>.

- [21] A. A. Adewale, A. Chik, O. k. Yusuff, S. A. Ayinde & Y. K. Sanusi, "First principle calculation of structural, electronic and optical properties of cds and doped $Cd_{x-1}A_xS$ (A=Co,Fe,Ni) compounds", *Materials Today Communications* **26** (2021) 101882. <https://doi.org/10.1016/j.mtcomm.2020.101882>.
- [22] M. Born, K. Huang & M. Lax, "Dynamical theory of crystal Lattice", *Am. J. Phys* **23** (1955) 474. <https://doi.org/10.1119/1/1934059>.
- [23] W. Voigt, "A determination of the elastic constants for beta quartz Lehrbuch der kristallphysik (bg teubner leipzig und berlin) 980 s", *Reproduced* **40** (1928) 2856. <https://doi.org/10.1103/PhysRev.62.395>.
- [24] A. Reuss, "Berechnung der fließgrenze von mischkristallen auf grund der plastizitätsbedingung für einkristalle", *ZAMM—Journal of Applied Mathematics and Mechanics/Zeitschrift für Angewandte Mathematik und Mechanik* **9** (1929) 49. <http://dx.doi.org/10.1002/zamm.19290090104>.
- [25] R. Hill, "The elastic behaviour of a crystalline aggregate", *Proceedings of the Physical Society* **65** (1952) 349. <https://doi.org/10.1088/0370-1298/65/5/307>.
- [26] D. H. Chung & W. R. Buessem, "The voigt-reuss-hill (VRH) approximation and the elastic moduli of polycrystalline ZnO, TiO₂ (rutile), and α -Al₂O₃", *Journal of Applied Physics* **39** (1968) 2777. <https://doi.org/10.1063/1.1656672>.
- [27] A. A. Audu, W. A. Yahya & A. A. Abdulkareem, "Ab-initio studies of the structural, electronic and mechanical properties of Zn_{1-x}Cr_xTe", *Physics memoir, Journal of theoretical and applied physics* **3** (2021) 38. <https://physicsmemoir.online>.
- [28] I. E. Igwe & Y. T. Batsari, "Atomistic simulation of the effect of temperature on mechanical properties of some nano-crystalline metals", *African Scientific Reports* **1** (2022) 95. <https://doi.org/10.46481/asr.2022.1.2.33>.
- [29] G. K. Madsen, J. Carrete & M. J. Verstraete, "BoltzTraP2: A program for interpolating band structures and calculating semi-classical transport coefficients", *Comput. Phys. Commun.* **231** (2018) 140. <https://doi.org/10.1016/j.cpc.2018.05.010>.
- [30] A. A. Adewale, A. Chik, T. Adam, T. M. Joshua & M. O. Durwoju, "Optoelectronic behavior of ZnS compound and its alloy: A first principle approach", *Materials Today Communications* **27** (2021) 102077. <https://doi.org/10.1016/j.mtcomm.2021.102077>.
- [31] M. Nabi & D. C. Gupta, "Potential lead-free small band gap halide double perovskites Cs₂CuMCl₆(MSb,Bi) for green technology", *Scientific Reports* **11** (2021) 12945. <https://doi.org/10.1038/s41598-021-92443-1>.
- [32] T. I. Al-Muhimeed, A. I. Aljameel, A. Mera, S. Saad, G. Nazir, H. Albalawi, S. Bouzgarrou, H. H. Hegazy & Q. Mahmood, "First principle study of optoelectronic and mechanical properties of lead-free double perovskites Cs₂SeX₆(XCl,Br,I)", *Journal of Taibah University for Science* **16** (2022) 155. <https://doi.org/10.1080/16583655.2022.2035927>.
- [33] M. A. Ali, A. H. Reshak, G. Murtaza, M. AL-Anazy, H. Althib, T. H. Flemban & J. Bila, "Optoelectronic and transport properties of Rb/Cs₂TeI₆ defective perovskites for green energy applications", *Int. J. Energy Res* **7** (2020) 1. <https://doi.org/10.1002/er.6378>.
- [34] N. I. Akpu, K. U. P. Okpechi, E. C. Nwaokorongwu, I. L. Ikhiyoa, J. C. Onwuzo, L. A. Nnanna & I. I. C. Agbodike, "Impact of temperature difference on the features of spray deposited yttrium doped cobalt selenide (YCoSe) thin films for photovoltaic application", *African Scientific Reports* **2** (2023) 143. <https://doi.org/10.46481/asr.2023.2.3.143>.
- [35] F. I. H. Alias, M. H. Ridzwan, M. K. Yaakob, C. W. Loy & Z. Mohamed, "Structural, electronic and optical studies of SrNiTeO double perovskite by first-principle DFT - LDA + U calculation", *Journal of Materials Research and Technology* **18** (2022) 1623. <https://doi.org/10.1016/j.jmrt.2022.03.017>.
- [36] Q. Mahmood, G. M. Mustafa, M. Morsi, H. Albalawi, T. H. Flemban, M. Hassan, H. Althib, M. I. Khan & T. Ghrib, "Theoretical investigations of optoelectronic and thermoelectric properties of halide based double perovskite halides: K₂TeX₆", *IOP publishing, Phys. Scr.* **96** (2021) 075703. <https://doi.org/10.1088/1402-4896/abfba8>.
- [37] A. B. Siad, M. Biara & M. B. Siad, "Structural mechanical optoelectronic and thermoelectric properties of double perovskite compounds Cs₂TeX₆(X=Br,I) for energy storage applications: First principles investigation", *Journal of Physics and chemistry of solids* **152** (2021) 109955. <https://doi.org/10.1016/j.jpccs.2021.109955>.
- [38] A. Menedjhi, N. Bouarissa, S. Saib, M. Boucenna & F. Mezrag, "Structure and optical spectra of double perovskite Cs₂AgBiBr₆ for solar cells performance", *ACTA Physica Polonica A.* **137** (2020) 1. <https://doi.org/10.12693/APhysPolA.137.486>.
- [39] Q. Mahmood, T. Ghrib, A. Rached, A. Laref & M. A. Kamran, "Probing of mechanical, optical and thermoelectric characteristics of double perovskites Cs₂GeCl/Br₆ by DFT method", *Materials Science in Semiconductor Processing* **112** (2020) 105009. <https://doi.org/10.1016/j.mssp.2020.105009>.
- [40] M. K. Zoubir, B. Fadila, B. Keltoum, A. Ibrahim, B. L. Farah, Y. Al-Douri & A. Mohammed, "Structural, electronic and thermodynamic investigation of Ag₂GdSi, Ag₂GdSn and Ag₂GdPb heusler alloys: First-principles calculations", *Materials Testing* **63** (2021) 537. <https://doi.org/10.1515/mt-2020-0088>.
- [41] M. A. Shah, M. A. Alam, A. Hossain, M. F. Hossain, M. Nuruzzaman, F. Parvin & M. A. K. Zilani, "Hydrostatic pressure on XLiH₃(X=Ba,Sr,Ca) perovskite hydrides: An insight into structural, thermo-elastic and ultrasonic properties through first-principles investigation" *Solid State Communications* **328** (2021) 114222. <https://doi.org/10.1016/j.ssc.2021.114222>.
- [42] N. Erum & A. Z. Iqbal, "Mechanical and magneto-opto-electronic investigation of transition metal based fluoro perovskites: An ab-initio DFT study", *Solid State Communications* **07** (2017) 1. <http://dx.doi.org/10.1016/j.ssc.2017.07.010>.
- [43] D. Pettifor, "Theoretical predictions of structure and related properties of intermetallics", *Materials Science and Technology* **8** (1992) 345. <https://doi.org/10.1179/MST.1992.8.4.345>.
- [44] S. F. Pugh, "Relations between the elastic moduli and the plastic properties of polycrystalline pure metals", *The London, Edinburgh, and Dublin Philosophical Magazine and Journal of Science* **45** (1954) 823. <https://doi.org/10.1080/14786440808520496>.
- [45] T. Takeuchi, "Conditions of electronic structure to obtain large dimensionless figure of merit for developing practical thermoelectric materials", *Materials Transactions* **50** (2009) 2359. <http://dx.doi.org/10.2320/matertrans.M2009143>.